Knotting spectrum of polygonal knots in extreme confinement

Claus Ernst
Department of Mathematics
Western Kentucky University
Bowling Green, KY 42101, USA

Eric J. Rawdon
Department of Mathematics
University of St. Thomas
Saint Paul, MN 55105, USA

Uta Ziegler
School of Engineering and Applied Sciences
Western Kentucky University
Bowling Green, KY 42101, USA

September 5, 2021

Abstract

Random knot models are often used to measure the types of entanglements one would expect to observe in an unbiased system with some given physical property or set of properties. In nature, macromolecular chains often exist in extreme confinement. Current techniques for sampling random polygons in confinement are limited. In this paper, we gain insight into the knotting behavior of random polygons in extreme confinement by studying random polygons restricted to cylinders, where each edge connects the top and bottom disks of the cylinder. The knot spectrum generated by this model is compared to the knot spectrum of rooted equilateral random polygons in spherical confinement. Due to the rooting, such polygons require a radius of confinement $R \geq 1$. We present numerical evidence that the polygons generated by this simple cylindrical model generate knot probabilities that are equivalent to spherical confinement at a radius of $R \approx 0.62$. We then show how knot complexity and the relative probability of different classes of knot types change as the length of the polygon increases in the cylindrical polygons.

1 Introduction

Many macromolecular chains live in a state of extreme confinement. For example, a single human cell contains roughly two meters of DNA. Virus heads also contain DNA packed

at almost unfathomable compaction. The P4 bacteriophage virus head, which is roughly spherical with diameter around 50 nm, contains 3 μm of double-stranded DNA [29] and gel electrophoresis shows that the DNA, upon circularization, forms very complex knots [2].

Polygons are often used as coarse grain models for macromolecular chains. As polygonal chains grow in length (i.e. number of edges), the probability of knotting approaches one [10, 36, 39]. Yet macromolecular chains, for example proteins [9], tend to contain less knotting than what one would expect based on length alone. The similarities and differences between natural systems and random models reveal clues into the mechanisms used to create and remove entanglement in natural systems.

The technique for generating random chains depends on what system one is trying to model. For example, wormlike chains [43] are used to model DNA and are typically generated using Monte Carlo methods with energy terms to give the chains some excluded volume and control local bending. Other terms can be added into the energy to simulate other conditions, such as confinement or supercoiling [31]. While knotting in spherical confinement has been studied using Monte Carlo techniques [3, 33, 34, 35, 42], it becomes increasingly difficult to simulate the chains under higher and higher levels of compaction.

In [11, 12, 13, 14, 15, 16, 17, 18], the authors (most of whom are authors on this paper) explored a direct method for generating knots in spherical confinement at levels of compaction that would be impractical using Monte Carlo methods. The idea was to explore how the confinement condition alone affects the knotting spectrum and the structure of the configurations as a function of length and confinement radius.

Unfortunately, even these direct generation methods have restrictions. In particular, the techniques of [7, 13] require that one vertex is at the origin – we say such a polygon is rooted at the origin. This restriction is necessary to compute the probability distributions that are used to sample the polygons. Using the two methods of [7, 13], one can sample uniformly from the set of unit-length edge equilateral polygons with any (possible) number of edges in any sphere of radius one or greater. However, unit-length edge equilateral polygons exist in any sphere of any radius $R \geq 1/2$. With that said, the case of R = 1/2 is not very interesting since the only possibility is that the polygons alternate between two antipodal points of the confinement sphere and, thus, all such polygons are degenerate. Thus, a new model is needed to study knotting in spheres of radii between 1/2 and one.

In this paper we explore extreme confinement, simulating the situation where the confinement radius is $R = 1/2 + \epsilon$ for some small $\epsilon > 0$. In this case the possible equilateral random polygons satisfy several properties: (i) each edge of the polygon has a length that is close to the diameter of the sphere; (ii) all vertices must be close to the boundary of the confinement sphere; (iii) if v_i , v_{i+1} , v_{i+2} , v_{i+3} are four consecutive vertices of a polygon, then v_i and v_{i+2} (and v_{i+1} and v_{i+3}) must be very close to each other; and (iv) if ϵ is small and the number of edges of the polygon is not too large, then the vertices with even indices and the vertices with odd indices are all close to two antipodal points, respectively, on the confinement sphere. Moreover, the polygons have even lengths. Thus for each polygon P there exists a cylinder C containing P whose top and bottom is capped by small spherical disks S_1 and S_2 whose centers are antipodal points on a confinement sphere. Note that if

we allow the length of the polygon (i.e. number of edges) to increase without bound, then of course such a cylinder C does not exist since the vertices for very long polygons can be close to any point on the confinement sphere.

To gain insight into the topological complexity of tightly confined polygons, we construct a simple model where the random polygons are nearly equilateral, lie within a cylinder, and can be generated easily. We take a fixed cylinder C = C(h, r) of radius r and height h with flat top and bottom disks D_1 and D_2 . We now connect points alternately from the disks D_1 and D_2 , with the points chosen with uniform probability with respect to area on each disk. The last point on D_2 is connected to the first point on D_1 to close the polygon. This simple method generates non-equilateral random polygons with even numbers of edges that are contained in the cylinder C. However, when h >> r the polygons are close to being equilateral. We do not claim that these cylindrical polygons have the exact probabilities as equilateral random polygons under tight spherical confinement. However, we believe we can gain insight into knotting in extreme confinement by analyzing these configurations when the number of edges in relatively small.

Next we want to understand how the relationship between the cylinder radius r and cylinder height h affects the spectrum of knot types of these polygons. Let us assume that r is fixed and h varies. For a given a set of vertices on the disks D_1 and D_2 and two different heights h and h', we can construct two polygons P and P' in the cylinders C(h,r) and C(h',r) respectively. Then P can be obtained from P' by a simple similarity, stretching or shrinking C(h,r) until C(h',r) is obtained. During this process no edges of P pass through each other and, thus, the polygons P and P' have the same knot type. Similarly, stretching or shrinking D_1 and D_2 by a similarity does not change the knot type of the polygon. Thus, the topological information is independent of the actual values of h and r.

Since the spectrum of knot types in this model is independent of h and r, the reader should worry that the model does not capture any information about knotting in spherical confinement with R close to 1/2. However, we show that the cylindrical model is consistent with our data from spherical confinement.

This manuscript is organized as follows. In Section 2 we provide some background information on knot theoretic concepts from this article and explain how our data set was generated. In Section 3 we argue that the polygons in the cylindrical model behave like spherically-confined polygons with a confinement radius smaller than one. In Section 4 we analyze the knot spectrum of the cylindrical polygons and compare it to the knot spectrum of the spherically-confined polygons. We conclude the article with Section 5 by summarizing the results and indicating future work.

2 Background

2.1 Knot theory background

To help those readers that are not familiar with knot theory, we outline and discuss briefly some topological concepts that are most relevant to this paper. For a more detailed exposi-

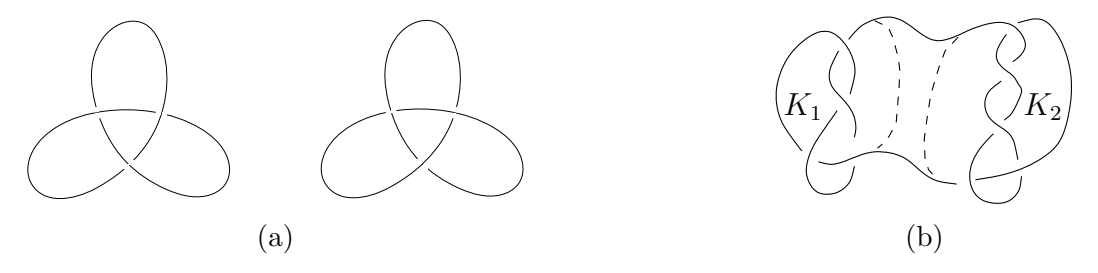


Figure 1: (a) A knot and its mirror image. (b) A composite knot constructed from two nontrivial knots K_1 and K_2 .

tion, please refer to a standard text on knot theory such as [1, 4, 30, 32].

A closed curve in \mathbb{R}^3 with no self-intersections is a $knot\ K$. In this paper, we concentrate on the subclass of knots which form space polygons with no self-intersections. Two knots are topologically equivalent if one can be continuously deformed (as continuous curves) to the other in \mathbb{R}^3 without being broken or causing self-intersection in the process. The class of all equivalent configurations is called a $knot\ type$. The knot type that contains a polygon representing the unit circle is called the $trivial\ knot\ (type)$, and is denoted 0_1 . Any configuration in the knot type 0_1 is called an unknot, or is said to be unknotted.

For a fixed knot configuration K in \mathbb{R}^3 , a regular projection of K is a projection of K onto a plane such that no more than two segments of K cross at the same point in the projection and endpoints of segments do not project onto other edges of the projection. An intersection in a regular projection is called a crossing. We typically draw a regular projection of K with the additional information that shows which strand passes over and which strand passes under at each crossing in the projection and call such a projection a knot diagram. The minimum number of crossings among all possible knot diagrams of a knot type K is called the crossing number of K and is denoted cr(K).

A knot diagram is alternating if the strands alternate between under and over at crossings as one travels along the curve. A knot type is alternating if it has an alternating diagram and is nonalternating if it does not have an alternating diagram. Note that nonalternating knots types have crossing number eight or greater. We obtain a diagram of the mirror image of \mathcal{K} if we switch the "over" and "under" at each crossing in a diagram of a knot type \mathcal{K} , see Figure 1(a).

A composite knot is a knot type that can be realized by connecting two nontrivial knots as shown in Figure 1(b). If a knot type is not composite, then it is a prime knot type. It is important to note that a composition of two nontrivial alternating knot types always admits a minimum knot projection that is alternating, as well as a minimum knot projection that is nonalternating. Thus, in our study the composite knots are not included in either of the alternating or nonalternating knot groups. Composite knot types have crossing number six or greater.

A knot type is *amphichiral* or *achiral* if a configuration of the given knot type is equivalent to its mirror image (in which case all configurations of the given knot type are equivalent to their mirror images). Through seven crossings, there are three prime amphichiral knot

types: 0_1 , 4_1 , and 6_3 . There are five prime 8-crossing and 13 prime 10-crossing amphichiral knot types. Knot types that are not amphichiral are called *chiral*.

In this paper, we explore the effect of knot complexity on the probability of different knot types and of groupings of knot types. Knot complexity can be measured in many different ways using quantities of classical knot theory (such as crossing number, genus, braid index, and bridge number) that can be found in any standard text on knot theory [1, 4, 30, 32]. In this article we use the crossing number as our measure of knot complexity since the crossing number is the most widely used measure of knot complexity and none of the alternatives seem to have any intrinsic advantage over the crossing number.

2.2 Generating polygons in cylindrical confinement

For this study, random polygons were generated with the number of edges ranging from six to 30 in steps of two. We call the number of edges in a polygon the *length* of the polygon. For each length, one million polygons were generated and analyzed. We begin at length six because all polygons with fewer than six edges are unknotted [38]. Our sampling ends at 30 because that is the smallest length where we cannot classify the knot types of over 50% of the samples. The data set of vertex coordinates and knot types of the random cylindrical polygons are posted at [21].

The data set polygons lie within a cylinder of unit radius and unit height, where the two endcap disks are parallel to the xy-plane and centered at the points (0,0,0) and (0,0,1). The vertices have (x,y)-coordinates chosen uniformly with respect to area on these disks and z-coordinates which alternate between 0 and 1. More specifically, for the x and y coordinates, it is easiest to think in terms of polar coordinates. One such x and y value is generated as follows: a double θ is chosen uniformly from $[0,2\pi)$ and a random double d is chosen uniformly from [0,1], both using the Gnu Scientific Library's gsl_rng_mt19937 as the random number generator [26]. Then $(x,y) = (\sqrt{d}\cos(\theta), \sqrt{d}\sin(\theta))$.

2.3 Classifying knot types

For each polygon (a total of 13,000,000 polygons), we classify the exact chiral knot type for almost all (more about this below) knot types with crossing number 16 or smaller. Knot types had been fully enumerated through 16 crossings [28] until just recently, when the limit was pushed to 19 crossings [5]. However, our tables only go through 16 crossings, which is why we stop there. If the crossing number of a configuration is greater than 16, we compute an upper bound for its crossing number. We implicitly assume that the crossing number of a composite knot is the sum of the crossing numbers of its factors, although that remains an open question [1].

Before we explain the details of the knot identification process, we summarize our assumptions used in the remainder of the paper:

1. If a knot configuration has crossing number 16 or smaller, we know the exact knot type without chirality (and with chirality, most of the time).

2. If the knot type is not classified as a 16 or smaller crossing knot type, then our computed crossing number upper bound is a good estimate of the actual crossing number.

For a given configuration, the knot identification process goes as follows:

- 1. We compute a crossing code for the configuration using software written by Rawdon.
- 2. We use Thistlethwaite's unraveller software [41] to simplify the crossing code, while keeping the knot type fixed.
- 3. We use Ewing and Millett's lmpoly software [24] to compute the HOMFLYPT polynomial [25, 37].
- 4. We look up the chiral knot types matching the given HOMFLYPT polynomial from a table computed by Rawdon.
- 5. We use knotfind, a portion of Hoste and Thistlethwaite's Knotscape [27], to compute a canonical simplified Dowker code from the simplified crossing code.
- 6. We look up the canonical simplified Dowker code in a table that exists as a part of Knotscape. This table provides the exact knot type, but without chirality information, so e.g. 3_1 instead of $+3_1$ or -3_1 .
- 7. We compare the output from (4) and (6) to compute the chiral knot type.

If the given configuration has a knot type with crossing number 16 or smaller, this process usually gives us the exact chiral knot type. However, if the HOMFLYPT polynomial does not appear in our table (implying that the knot type has a crossing number exceeding 16) or a component of our software chain fails (which only occurs with knotfind), we do additional detective work.

In some cases, the software knotfind can fail. If this happens and the HOMFLYPT polynomial of the configuration is found in our HOMFLYPT table, we compute the isometry signature [19] of the configuration using SnapPy [8]. The isometry signature is a complete knot invariant (but without chirality information, similar to knotfind), but is only defined for knot types whose exteriors are cusped hyperbolic manifolds. While this is imperfect (for example, composite knot types are not cusped hyperbolic manifolds), it allows us to classify the knot types of some additional configurations by comparing the isometry signature to a table computed by Rawdon using SnapPy.

If after these computations we have not found the knot type, we believe that the knot type has crossing number 17 or greater. In those cases, the output from unraveller provides an upper bound on the crossing number of the given knot type. To maximize the probability that we have the actual crossing number, we also try to simplify the crossing code using the command simplify in SnapPy. In most cases, the results from both programs agree. We use the minimum of the results of the two computations to be our estimate of the crossing number. If this estimate is 17 and the HOMFLYPT polynomial does not appear in our

table, then we know that the crossing number really is 17. Beyond 17 crossings (or if the HOMFLYPT polynomial does appear in our table and neither knotfind nor the isometry signature is able to identify the knot type), we cannot guarantee that we have the correct crossing number, although we have no reason to believe that the computations somehow fail beyond 17.

It is important to note that we had no cases where the knot could be simplified to 16 or fewer crossings and we did not identify the knot type.

There is one more peculiarity in this process. The software knotfind attempts to decompose composite knots if the composition is easily seen in the projection. We use this functionality recursively to attempt to factor a knot into its prime knot factors. If the crossing number of the composite knot does not exceed 16, then we determine the knot type as described above. However, if the crossing number of a composite knot exceeds 16, yet each of the prime factors has crossing number not exceeding 16 then we identify the prime knot types of the factor knots. The net result is that for some configurations which form composite knots with crossing number greater than 16, we still can compute their knot type (e.g. $7_1\#10_2$). In these cases, we do not compute the chiralities of the factors. There is no guarantee that knotfind always decomposes composite knots.

If the crossing number of the knot type is 16 or smaller, this process provides the chiral knot type of the configuration with one caveat. There are some chiral knot types for which both chiralities have the same HOMFLYPT polynomial, e.g. the 9_{42} knot. For those knot types, both chiralities are grouped together. There are 5344 such prime knot types (one 9-crossing, five 10-crossing, two 11-crossing, 91 12-crossing, 35 13-crossing, 616 14-crossing, 395 15-crossing, and 4199 16-crossing) and 463 composite knot types containing one of these knot types.

We end our data gathering at a length of 30 edges because that is when the knot configurations with more than 16 crossings becomes over half of the population. We call those configurations *unclassified*, which also includes the composite knot types which **knotfind** was able to classify with crossing number exceeding 16.

3 Comparison with earlier results on confined polygons

Since the cylinders can be stretched while retaining the same knotting distribution, one might ask whether these knots even behave as though they are confined. In this section, we argue that the cylindrical knot model is a good approximation of knotting under spherical confinement with a radius significantly smaller than one. We have studied knotting of equilateral random polygons under spherical confinement [11, 12, 13, 14, 15, 16, 17, 18] concentrating on how the confinement radius R and/or the polygon length L (i.e. the number of edges) influence knot complexity. However, in order to generate these polygons directly, recall that the polygons needed to be rooted (i.e. have one vertex at the origin).

We compare the cylinder polygon data generated for this paper (which has 1,000,000

samples for even lengths between six and 30) to data generated in the above-mentioned papers. There are two such data sets. First, for $R \in \{1.0, 1.1, \dots, 2.9, 3.0, 3.5, 4.0, 4.5\}$ and length values between 10 and 90 by steps of 10, we have 10,000 configurations for most (L, R) pairs (we did not compute the knot types of the configurations for some of the mostly highly confined pairs because we could classify so few knot types). Second, for length 30 and the same R values, and for R = 3.0 and the same length values, we have 100,000 configurations. We call these rooted data sets spherical data set 1, with 10,000 samples per (L, R) pair, and spherical data set 2, with 100,000 samples per (30, R) and (L, 3.0) pair. The vertex coordinates and corresponding knot types for these two data sets are posted at [22, 23].

The goal of the following subsections is to determine how the cylindrical and the two rooted spherical polygon data sets align. In particular, is there evidence that the cylindrical polygons behave as if they are in tighter confinement than the spherical polygons?

We compare the cylindrical and spherical data in various ways: by measuring the mean topological complexity (Section 3.1), by analyzing the probabilities of different classes of knot types (Section 3.2), and by computing the relative probabilities of knot types within some fixed crossing numbers (Section 3.3).

3.1 Mean topological complexity

We measure the change in the complexity of the configurations by computing the mean topological crossing number, i.e. the average of the crossing numbers of the configurations. In Figure 2(a) we show the mean topological crossing number of the cylindrical polygon configurations, both including the unknotted configurations and excluding them. In Figure 2(b), we include the maximum observed (estimated) crossing number, the highest (estimated) crossing number observed with at least 10 samples, and the (estimated) crossing number appearing at the 99.99% percentile. With the exception of Figure 2(b), we include error bars in all graphs in this article. Most of the time, the error bars are so small that they can barely be seen.

In Figures 3 and 4, we present a combination of data from spherical data sets 1 and 2, and the cylindrical data related to the mean topological complexity. In Figure 3(a), we compare the mean topological complexity of the cylindrical data with the spherical set 1 data. Note that the spherical data graphs are ordered by the confinement radius and it is heartening to see that the cylindrical data behaves as being significantly more confined than the spherical data, even at R = 1. The question is: can we estimate a radius R_0 at which the cylindrical data is consistent with the extension of the spherical data to R_0 ?

We begin by using our most reliable spherical data, which comes from spherical data set 2 for length 30 and contains 100,000 configurations for each analyzed radius. Figure 3(b) shows the mean topological crossing number with confinement radii R=1 through R=4.5 for data including the unknots (100,000 configurations) and excluding the unknots (sample size depends on R). Each point set is fit with a function of the form $ae^{bx} + c$. Table 1 shows the computed fit parameters, the computed expected value (E) for mean topological crossing number in the cylindrical model, and the radius value (X) at which the fit function passes through the value E. Based on Table 1, we decided to use two digits beyond the decimal

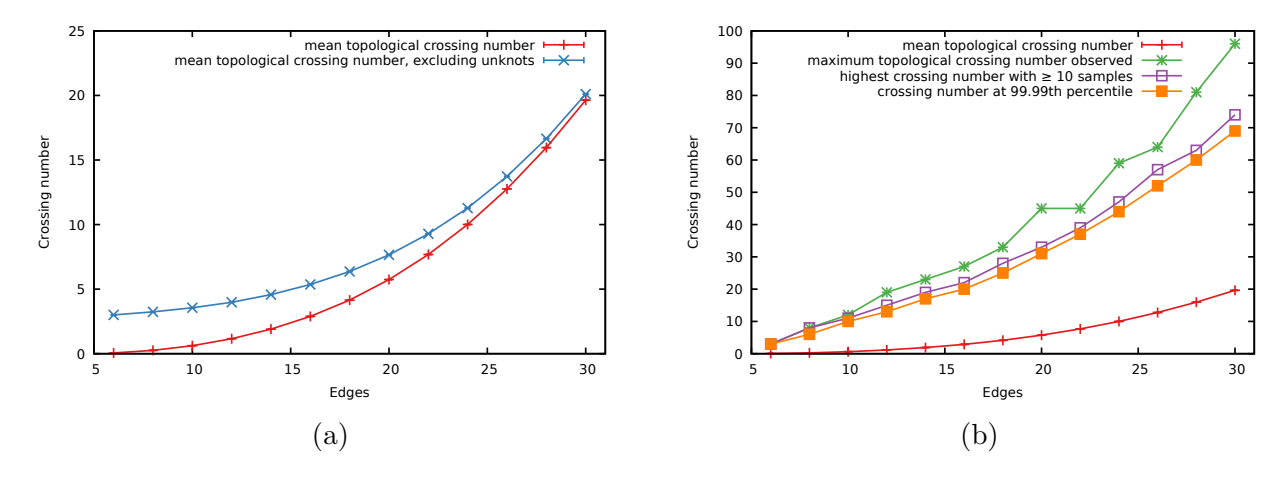


Figure 2: (a) Mean topological crossing number, including and excluding unknots, for the cylindrical data. (b) Maximum observed (estimated) crossing number, highest (estimated) crossing number with 10 or more samples, and the (estimated) crossing number at the 99.99th percentile for the cylindrical data.

point and chose $R_0 = 0.62$ since it is between the two X values of 0.6289 and 0.6160. The next question is: does this estimate of $R_0 = 0.62$ also match our other data?

Figure 4 shows the mean topological crossing number for 10 and 20 edges and radii $1.0 \le R \le 4.5$ from spherical data set 1, which has 10,000 configurations per (R, L) pair when we include unknots. We fit each of the data sets, with and without unknots independently, again using functions of the form $ae^{bx}+c$, and include the cylindrical data point at $R_0=0.62$. The fit parameters are in Table 1. In the graphs, the fitting functions pass through the cylindrical data points when the unknots are included. When the unknotted configurations are not included, the cylindrical data points do not lie exactly on the fitting graph. However, the X values in Table 1 for these situations (0.5861 and 0.6994) are still within 13% of $R_0=0.62$ despite the considerably smaller data sets (see the Min N and Max N columns).

Figures 3 and 4 show that, with respect to mean topological crossing number, cylindrical polygons behave consistent with the data for polygons under spherical confinement extended to a radius $R_0 \approx 0.62$. In the following subsections, we analyze whether this behavior extends to probability data.

3.2 Probabilities of classes of knot types

In Figure 5, we analyze the relative probabilities of different classes of knot types at L=30 from spherical data set 2. Figure 5(a) shows the plots for the unknots, alternating prime, nonalternating prime, composite, and unclassified knot types with the cylindrical data shown at $R_0=0.62$. The cylindrical data and spherical data for $R\leq 1.5$ is shown in Table 2 under "Raw percent". Unfortunately, the unclassified knot types dominate the cylindrical population, making it difficult to predict the relative probabilities of the other classes in the cylindrical model.

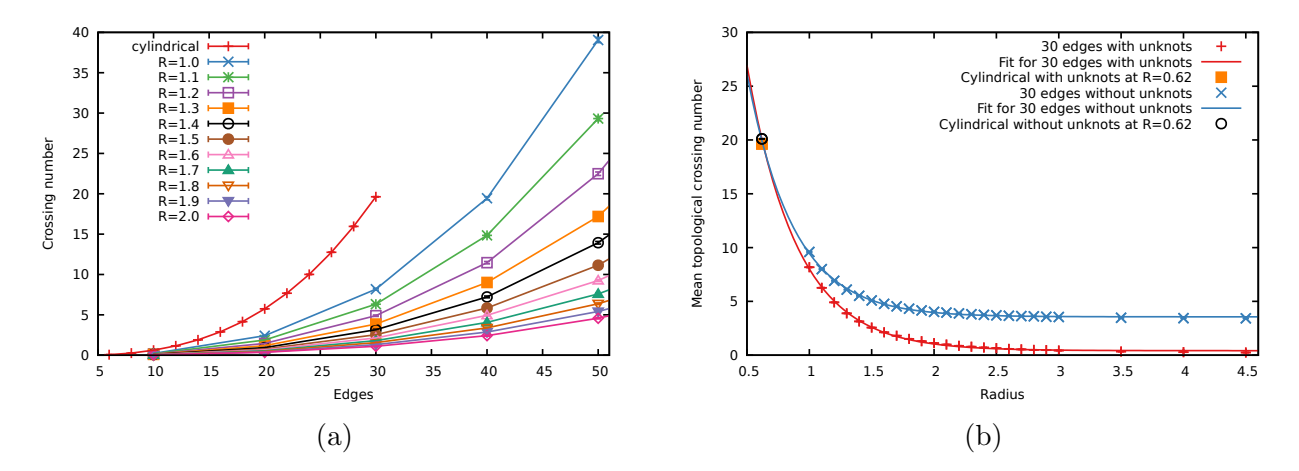


Figure 3: (a) Mean topological crossing number (including unknots) for the cylindrical data and for spherical confinement radii $1.0 \le R \le 2$ and lengths $6 \le L \le 50$ from spherical data set 1. (b) Mean topological crossing number, including and excluding unknots, for 30-edge polygons at radii $1.0 \le R \le 4.5$ from spherical data set 2. The fitting functions, of the form $ae^{bx} + c$, from Table 1 are shown along with the mean topological crossing number for the cylindrical data placed at $R_0 = 0.62$.

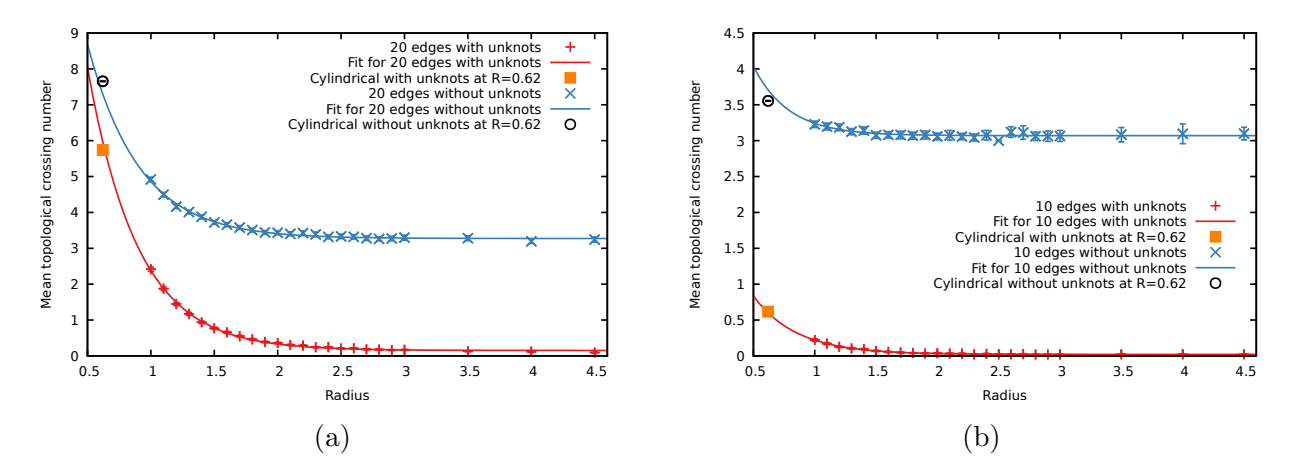


Figure 4: (a) Mean topological crossing number, including and excluding unknots, for 20-edge polygons. (b) Mean topological crossing number, including and excluding unknots, for 10-edge polygons. Both graphs are based on data from spherical data set 1. The fitting functions, of the form $ae^{bx} + c$, from Table 1 are shown along with the mean topological crossing number for the cylindrical data placed at $R_0 = 0.62$.

Table 1: Table of fitting values for Figures 3(b) and 4, both including and excluding unknots, for the mean topological crossing number of the spherical data. The mean topological crossing number values were fit by functions of the form $ae^{bx} + c$ for fixed length values and varying radii. The first column shows the length. The second column shows whether the unknotted configurations are included for this fit. The next three columns show the computed fitting values. The E column is the computed mean topological crossing number for the cylindrical data. The X column shows the x value where $ae^{bx} + c = E$, i.e. the spherical radius corresponding to E based on the fitting function. The number of configurations used to compute the mean topological crossing number varies greatly depending on whether we include or exclude unknots and whether we are using spherical data set 1 versus 2. For L=30, the data comes from spherical data set 2 with 100,000 configurations per radius when including the unknots. For L=20 and L=10, the data comes from spherical data set 1 with 10,000 configurations per radius when including the unknots. The last two columns (Min N and Max N) show the minimum and maximum number of configurations used to compute the mean topological crossing data points within the given class of data. For example, for L=30 when the unknots are not included, the data size ranges from 85, 145 configurations at R = 1.0 to 7,275 at R = 4.5. Because our data is much more robust for L=30 than for L=10 and L=20, we chose $R_0=0.62$ based on the average X value (to two digits) for L=30.

L	unknots?	a	$\mid b \mid$	c	$\mid E \mid$	X	Min N	$\operatorname{Max} N$
30	yes	92.6351	-2.50150	0.419792	19.63	0.6289	100,000	100,000
30	no	86.6144	-2.68784	3.56612	20.11	0.6160	7275	85,145
20	yes	27.9923	-2.53166	0.151451	5.74	0.6365	10,000	10,000
_20	no	18.4617	-2.45392	3.27287	7.66	0.5861	288	4908
10	yes	3.32472	-2.82008	0.0210849	0.62	0.6097	10,000	10,000
10	no	5.39080	-3.44447	3.06999	3.55	0.6994	71	685

In Figure 5(b), we redistribute the unclassified knots for the spherical data when $R \leq 1.5$ and for the cylindrical data to approximate what Figure 5(a) might look like without the unclassified configurations. Table 2 shows some of the data plotted in Figure 5(a) and Figure 5(b). In particular, note the "unclass" column, i.e. the percentage of unclassified knot types, whose values we would like to redistribute to the other categories. Recall that the unclassified knot types are prime and composite knot types with crossing numbers of 17 or greater. As such, we do not assign any of the unclassified knots to the unknots category.

In Table 3, we show the breakdown by category for 16, 15, and 14-crossing knot types for the spherical data when $R \leq 1.5$ and the cylindrical data. Note that the sample sizes within this data are small, but there are still lessons to be learned. Looking at the rows, we see that the 16-crossing knot types have the lowest percentage of alternating knot types and the highest percentage of nonalternating knot types. The percentages of composite knot types also generally are the lowest for 16 crossings.

This information suggests that the unclassified cylindrical knot types have fewer than 2.34% alternating prime knot types, greater than 92.29% nonalternating prime knot types, and fewer than 5.37% composite knot types. Since the great majority are nonalternating, we adjust the cylindrical knot classes by splitting the 59.16% of unclassified knot types based on the relative percentages for the 16-crossing knot types: namely, 2.34% of the 59.16% are assigned to the alternating prime category, 92.29% of the 59.16% to the nonalternating prime category, and 5.37% of the 59.16% to the composite category. Note that we could have assigned a higher percentage to the nonalternating category (since the data shows that the percentage of nonalternating knots is growing with crossing number) and lower values to the alternating and composite categories, although the differences would barely be noticeable on the graph. We adjust the categories for the spherical data analogously using the 16-crossing data from Table 3, as shown in the adjusted percent columns of Table 2.

The graphs of the adjusted values in Figure 5(b) are shown with cubic splines fit to the data. What can we learn from this figure? First, for these groupings of knot types, the cylindrical data is consistent with the spherical data at a radius value $R_0 \approx 0.62$. Second, we can conjecture on the behavior of length 30 polygons as R approaches 0.5. Our overall assumption here is that there are no radical changes between R = 0.5 and the rest of the data. It could be the case that the knotting spectrum changes quickly as $R \to 0.5^+$, although we have no such evidence and no argument for why that would be the case.

The unknots appear to be approaching a probability of 0 as $R \to 0.5^+$, although it is possible that the limiting probability is strictly greater than 0. If that is the case, we would expect that this is a small-length phenomenon and that when the lengths are longer, the unknot probability approaches 0 as $R \to 0.5^+$.

The nonalternating knot types increase in probability as $R \to 0.5^+$. The spline fit between R = 0.62 and R = 1.0 suggests that there is an inflection point between these two values, which would likely provide a value around 0.8 as $R \to 0.5^+$.

The probability of alternating knot types decreases as $R \to 0.5^+$. Based on the spline fit between R = 0.62 and R = 1.0, it seems unlikely that the probability would approach 0. It seems more likely that there is an inflection point between R = 0.62 and R = 1.0 and that

Table 2: Percentages of unclassified (unclass), alternating prime (alt), nonalternating prime (non), and composite (comp) knot types at L=30 for the cylindrical polygons and for the spherical data set 2 polygons with $1.0 \le R \le 1.5$. In Figure 5(b), we redistribute the unclassified knot types to the other categories based on the relative percentages for 16-crossing knot types shown in Table 3, except for the unknot counts. The table shows the measured (raw) percentages along with the adjusted percentages plotted in Figure 5(b) for the tightest confinements.

		Raw	percen	Adjusted percent					
\overline{R}	unclass	unknot	alt	non	comp	unknot	alt	non	comp
cyl	59.16	2.36	14.47	20.47	3.54	2.36	15.85	75.07	6.72
1.0	9.06	14.86	43.05	26.47	6.57	14.86	43.14	35.09	6.92
1.1	3.67	21.65	47.96	20.57	6.17	21.65	47.98	24.05	6.32
1.2	1.53	29.04	49.31	14.57	5.55	29.04	49.31	16.01	5.63
1.3	0.57	36.07	48.87	9.96	4.52	36.07	48.87	10.51	4.54
1.4	0.25	43.15	46.37	6.60	3.62	43.15	46.37	6.85	3.62
1.5	0.11	49.58	42.92	4.47	2.94	49.58	42.92	4.57	2.94

the limiting value is around 0.12. The estimation for alternating knot types is likely a bit high. However, even if we assume that none of the unclassified knot types are alternating knot types (this is essentially the case in Figure 5(a)), it still appears that the limiting value would be around 0.08.

For the composite knot types, with $R=0.62,\,1.0,\,1.1,\,$ and 1.2, the probability values are 6.72%, 6.92%, 6.32%, and 5.63%, respectively. It is unclear if the slightly lower value at R=0.62 versus R=1 is real, or numerical error, or error in our adjustment assumptions. It seems that there are two possibilities: 1) the composite knot type percentage increases as $R\to 0.5^+$, approaching an asymptotic value around 7%, or 2) the percentage of composite knots decreases as $R\to 0.5^+$ with a peak somewhere between R=0.62 and R=1.1, tending to a limiting value around 0.065. We see a slight decrease like this again in Section 4.1. As such, we would conjecture that the latter property holds, i.e. that the limiting value is around 0.065.

Next we analyze probabilities when we group together knot types with the same crossing number. We begin by graphing the probabilities as a function of length for the cylindrical polygons and spherical polygons of set 1 with R values between 1.0 and 1.8 by steps of 0.2 (which was done simply to provide some separation between the graphs). Figure 6 shows the probability graphs for just the 0_1 and just the 3_1 knot types (the only knot types with crossing numbers 0 and 3, respectively). Figure 7 shows the probability graphs when we combine all 5-crossing knot types and combine all 6-crossing knot types. Again the cylindrical data behaves similar to the spherical data at a confinement radius smaller than 1.0, although there is no easy way to glean an approximated R value.

Alternately, we can view the probability values as a function of radii for various lengths, see Figures 8 and 9. For these graphs, we include the cylindrical values at R = 0.62 and find

Table 3: Percentages of alternating prime (alt), nonalternating prime (non), and composite (comp) knot types with fixed crossing numbers for L=30. The data is shown for crossing numbers 16, 15, and 14 within the cylindrical data (cyl) and spherical data set 2 with radii $1.0 \le R \le 1.5$. The P columns show the percentages of the 100,000 configurations with the given number of crossings.

		16 crc	ssings			15 crc	ssings		14 crossings			
\overline{R}	alt	non	comp	P	alt	non	comp	P	alt	non	comp	P
cyl	2.34	92.29	5.37	3.95	4.30	89.76	5.93	4.03	7.77	84.95	7.28	3.73
1.0	0.96	95.16	3.88	2.40	1.60	94.30	4.10	3.07	3.63	90.26	6.10	3.44
1.1	0.60	95.18	4.22	1.33	1.49	93.73	4.78	1.88	3.11	91.39	5.49	2.18
1.2	0.15	94.59	5.26	0.67	1.04	94.90	4.06	0.96	2.50	91.36	6.14	1.24
1.3	0.33	96.03	3.64	0.30	0.77	93.45	5.78	0.52	2.07	91.73	6.20	0.68
1.4	0.00	97.87	2.13	0.14	0.47	95.75	3.77	0.21	1.12	94.10	4.78	0.36
1.5	0.00	95.59	4.41	0.07	1.49	97.01	1.49	0.13	2.58	92.78	5.43	0.13

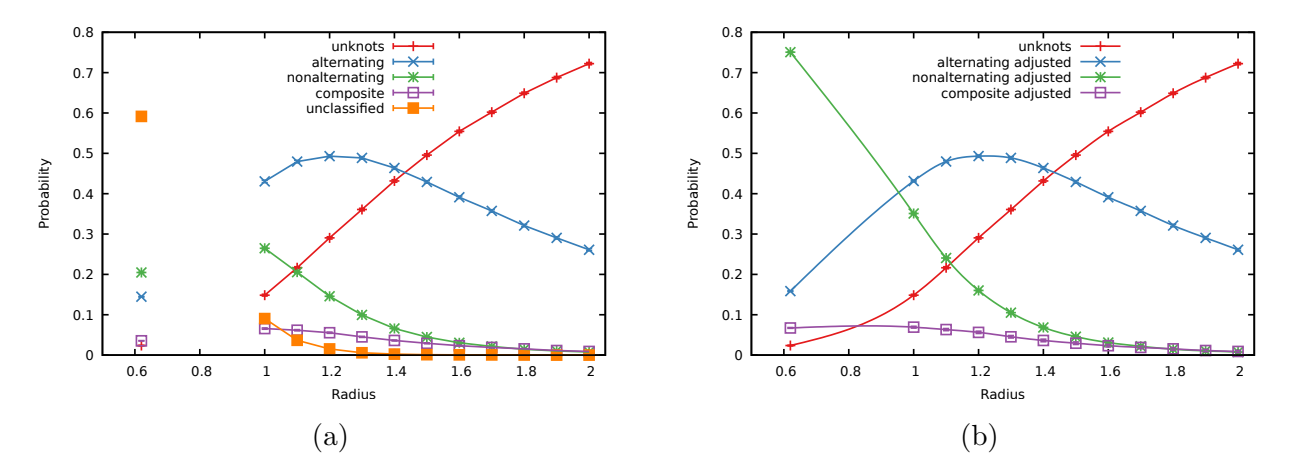


Figure 5: (a) The split between unknots, alternating prime, nonalternating prime, composite, and unclassified knot types for length 30 polygons with different radii from spherical data set 2 along with the cylindrical data placed at $R_0 = 0.62$. (b) We split the unclassified knot types (as described in the text) to obtain an approximation of what the length 30 data might look like without the unclassified knot types, and fit that data with cubic splines.

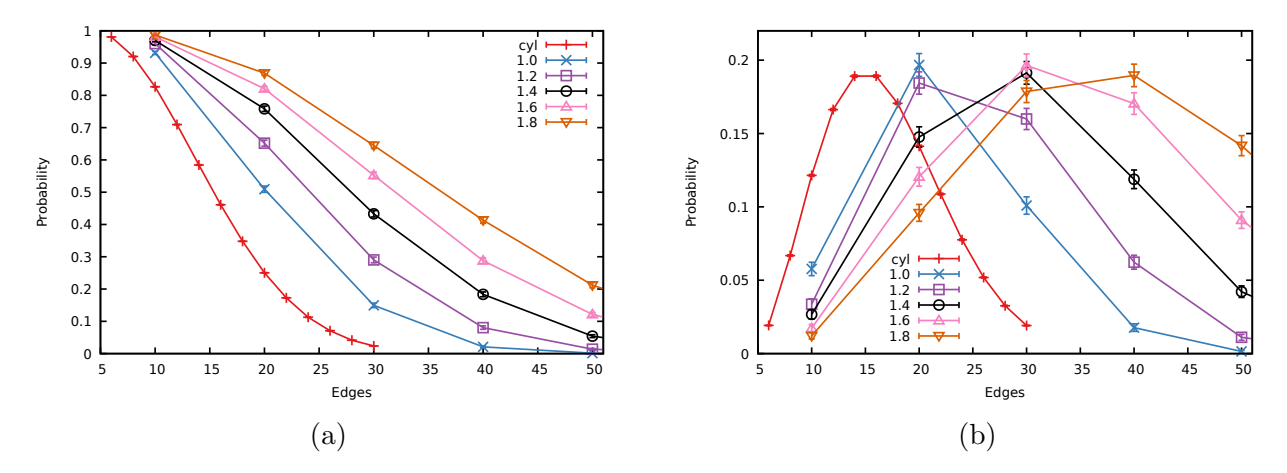


Figure 6: The spherical data set 1 probabilities of the (a) unknot 0_1 and (b) trefoil 3_1 as a function of length for various R values together with the cylindrical data.

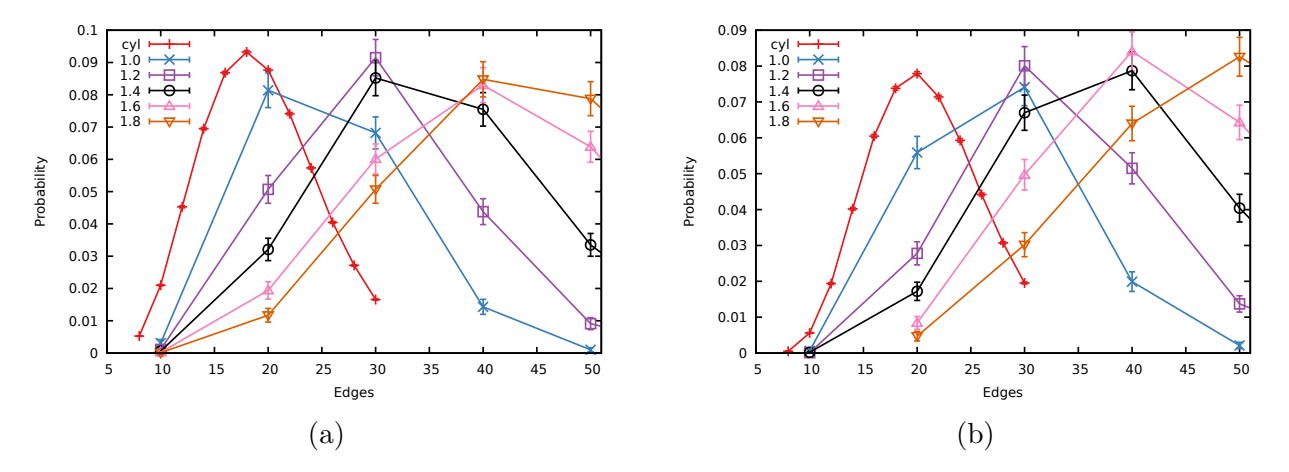


Figure 7: The spherical data set 1 probabilities of (a) 5-crossing and (b) 6-crossing knot types as a function of length for various R values together with the cylindrical data.

that the values, again, are consistent with the spherical data.

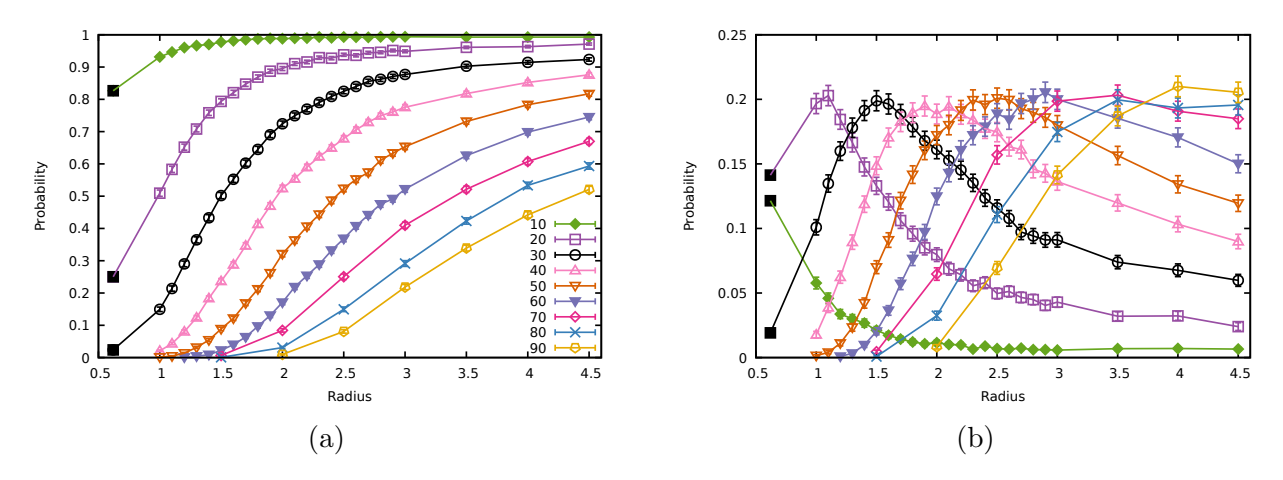


Figure 8: The spherical data set 1 probabilities of the (a) unknot 0_1 and (b) trefoil 3_1 as a function of radius for various lengths together with the cylindrical data plotted at $R_0 = 0.62$.

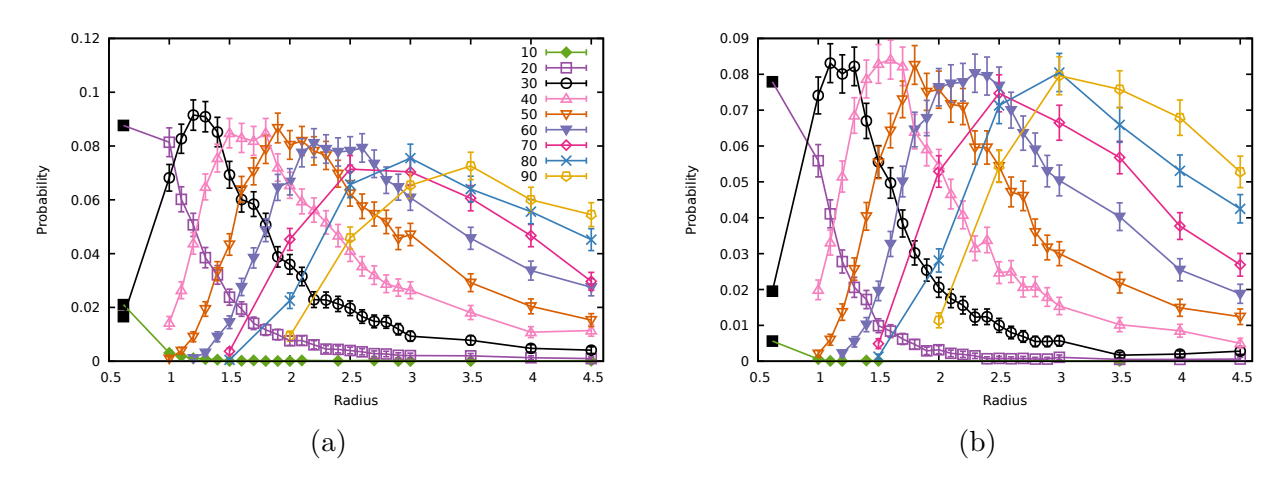


Figure 9: The spherical data set 1 probabilities of the (a) 5-crossing and (b) 6-crossing knot types as a function of radius for various lengths together with the cylindrical data plotted at $R_0 = 0.62$ for lengths 10, 20, and 30.

3.3 Relative probabilities of individual knot types with a given crossing number

In [16, 18], we analyzed the relative probability of different knot types within a given crossing number under spherical confinement. In particular, we observed that the relative probability of different knot types is largely independent of the strength of confinement and, to a lesser extent, also independent of length (provided the length is sufficiently large). Here we provide some examples including the cylindrical data.

In this analysis, we group mirror images together and compute the relative probabilities of individual knot types within a given crossing number. For example, there are five knot types with crossing number six, namely 6_1 , 6_2 , 6_3 , $3_1#3_1$, and $3_1#m3_1$ (where m denotes the mirror chirality). We compute the probabilities of these five knot types relative to the sum of these probabilities. This means that in each figure the probability values of all curves for the same confinement-value add up to one. Figure 10 shows the relative probability data for 6-crossing and 7-crossing knot types at L=30 and varying R values. The data for L=30 from R=1 to R=2 comes from spherical data set 2 and the leftmost point is from the cylindrical polygons. We note that the percentage of 3.1#3.1 knot types is essentially equal to the percentage of 3.1 # m3.1 knot types in the cylindrical data in Figure 10(a). Similarly, Figure 11 shows the data for the 8-crossing composite and nonalternating knot types. While the cylindrical data point really could be set at any 0.5 < R < 1 value, we use R = 0.62 to be consistent with earlier graphs. Note that the relative probability heights and orderings, considering the size of the error bars, are consistent between the cylindrical data and the spherical data. Also, note that the percentage of 3.1#5.1 (or 3.1#5.2) knot types is essentially equal to the percentage of 3.1 # m5.1 (or 3.1 # m5.2) knot types in cylindrical data in Figure 11(a).

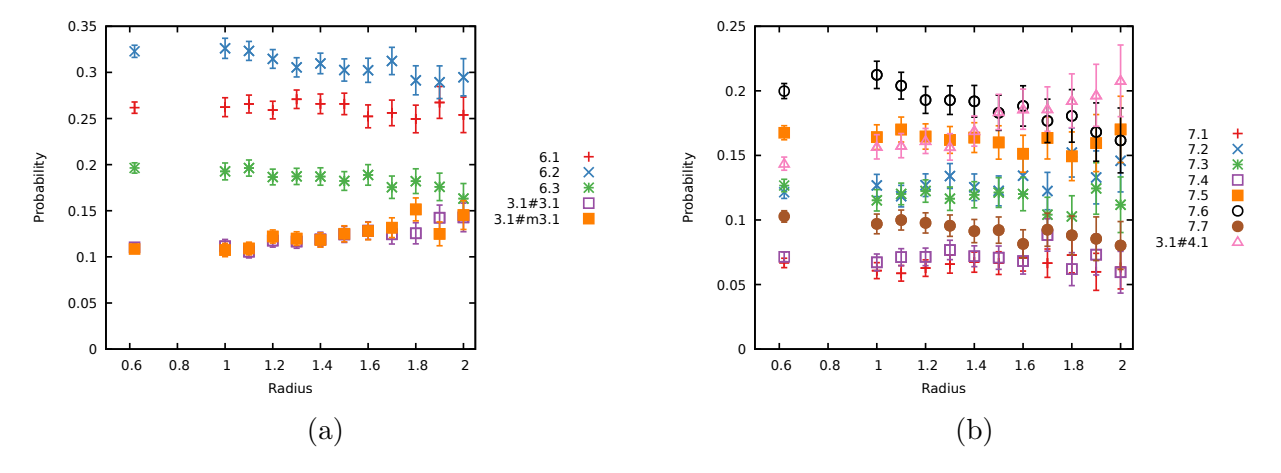


Figure 10: The relative probabilities of (a) 6-crossing and (b) 7-crossing knot types for length 30 polygons at different radii from spherical data set 2 together with the cylindrical data plotted at R = 0.62.

3.4 Conclusion

The cylindrical polygon data is consistent with spherical data at a confinement radius smaller than 1. More specifically, the cylindrical data is consistent with a spherical confinement radius of approximately $R_0 = 0.62$.

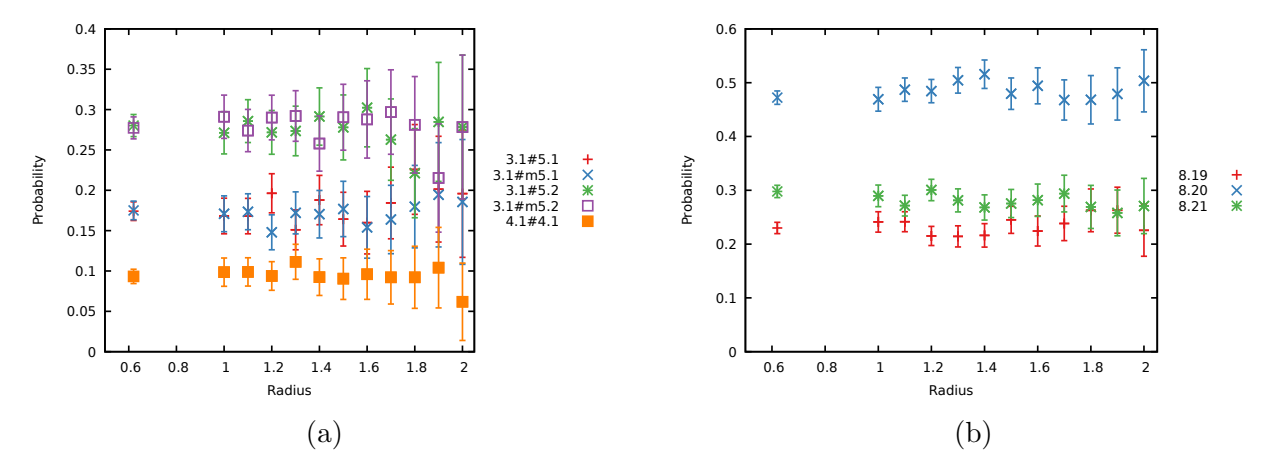


Figure 11: The relative probabilities for (a) 8-crossing composite and (b) 8-crossing nonalternating knot types for length 30 polygons at different radii from spherical data set 2 together with the cylindrical data plotted at R = 0.62.

4 The knot spectrum of cylindrical polygons

Now that we have established that the cylindrical polygons behave like spherical polygons under tight confinement, our goal is to explore knotting complexity and different classes of knot types as a function of length. Furthermore, we speculate on what one might expect as the length grows without bound.

4.1 Probabilities of classes of knot types

Figure 12(a) shows the probability of unknots, prime alternating knot types, prime nonalternating knot types, composite knot types, and unclassified knot types as a function of length for the cylindrical polygons. Note that we can only separate the prime knots from the composite knots when the crossing number is 16 or smaller. We see the prime alternating knot types and prime nonalternating knot types reach local maxima within the range of edges. However, the population of unclassified knot types increases to nearly 60% of our population at L=30, so it is difficult to decipher whether these behaviors are real.

To provide some clarity, we divide the unclassified knots by estimating how many of the unclassified configurations are prime alternating, prime nonalternating, and composite (similar to what we did earlier for mean topological crossing number). In Table 4, we show the number of unclassified configurations (out of 1,000,000 samples per number of edges) along with the percentage of alternating prime, nonalternating prime, and composite knot types within the populations of knot types with crossing numbers 16, 15, and 14. Recall that the unclassified knots have crossing number 17 and higher. As in Section 3.1, we use the relative percentages of these populations at 16 crossings to reassign the unclassified configurations. For example, at 26 edges, 2% of the 294,759 unclassified knots are added to the alternating prime knots, 94% are added to the nonalternating prime knots, and 4%

are added to the composite knots (although we do not round off the percentages). The table shows that, for a fixed length, the percentage of alternating prime and composite knot types decrease with increasing crossing number and the percentage of nonalternating prime increases with increasing crossing number. Thus, these estimations likely slightly overcount prime alternating and composite knots and undercount nonalternating prime knots. Since the percentages of prime alternating knot types and composite knot types are small (between 0% and 5%), these small amounts of overcounting and undercounting result in minimal changes in the graphs.

Figure 12(b) shows the probability of the different classes after these reassignments. There are several lessons here. We see the unknots approaching an asymptotic value of 0, which we would expect since the probability of unknotted configurations approaches 0 with increasing confinement pressure (see Figure 8(a)). The nonalternating knot types dominate at long lengths. The alternating prime knots reach a peak at length 18. Since the adjustments for prime alternating knot types appear to be overestimations, this peak is real. Asymptotically, we would expect the prime alternating graph to continue to decrease. It is not clear if the alternating prime knots approach a probability of 0 or some positive number.

The composite knot data is also ambiguous. For lengths 24, 26, 28, and 30, the adjusted values are 6.28%, 6.63%, 6.80%, and 6.72%, respectively. Like we saw in Section 3.2, it is unclear if the slightly lower value at L=30 versus L=28 is real, or numerical error, or error in our adjustment assumptions. Again, it seems that there are two possibilities: 1) the composite knot type percentage increases with L, approaching an asymptotic value around 7%, or 2) the percentage of composite knots decreases after length 28 (or somewhere near there), tending towards some asymptotic value (which could be 0 or non-zero). We attempted to address this issue, but ultimately could not find any compelling evidence one way or the other. Since we see this same behavior for fixed length and varying R, we lean towards believing that the percentage of composite knots does decrease after length 28.

In short, our data does not address the asymptotics of the alternating prime and composite knot types. If we had to guess, we would conjecture that the prime alternating knot types approach a probability of 0 and the composite knot types approach a probability of around 0.065.

4.2 Probabilities for fixed crossing numbers

For a given number of crossings, what would we expect for the probability curve in the cylindrical confinement model as length increases? There are different factors at play which restrict and encourage knotting of different levels of complexity.

First, for a knot type, or fixed number crossings (or, knot types with bounded crossing number like in Figure 12(a), or really, any finite set of knot types), we expect the probability to approach 0 as the number of edges tends to infinity. In particular, suppose we have a (2n)-gon and we add two more edges to create a (2n+2)-gon. Those two extra edges are likely to pierce several triangles created by other pairs of consecutive edges and create many new crossings. When n is large, it is difficult for these new crossings to be all nugatory crossings or to "undo" some of the knotting from other edges (which would likely be a very

Table 4: Within the cylindrical configurations, the number of unclassified knot types (unclass) along with the percentages of alternating prime (alt), nonalternating prime (non), and composite (comp) knot types at different lengths for crossing numbers 16, 15, and 14. The N columns show the number of configurations (out of the 1,000,000 samples) with the given number of crossings. This table shows the non-adjusted values.

		16 crossings					15 d	crossing	s	14 crossings			
\overline{L}	unclass	alt	non	comp	N	alt	non	comp	N	alt	non	comp	N
12	2				0				0				0
14	96	0	100	0	87	0	100	0	249	0	99	1	440
16	1240	0	99	1	949	0	99	1	1714	1	98	1	2574
18	7903	0	99	1	3987	0	98	2	6391	1	96	2	8360
20	29573	0	98	2	10916	1	97	2	15321	2	94	3	18565
22	80364	1	97	3	21729	2	95	3	27721	4	92	4	30799
24	168878	1	95	4	33127	2	94	4	39366	5	90	5	41677
26	294759	2	94	4	41236	3	92	5	45853	6	88	6	46499
28	442976	2	93	5	43852	4	91	5	45854	7	87	7	44267
30	591562	2	92	5	39525	4	90	6	40283	8	85	7	37285

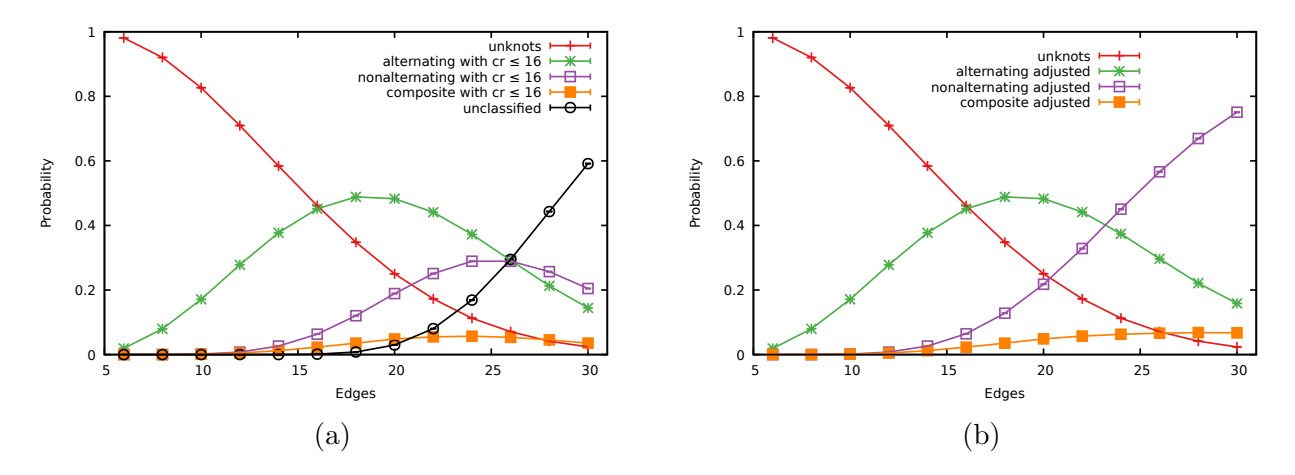


Figure 12: (a) Probabilities of unknots, prime alternating knot types, prime nonalternating knot types, composite knot types, and unclassified knot types for all lengths from the cylindrical data. (b) We split the unclassified knot types (as described in the text) to obtain an approximation of what the cylindrical data might look like without the unclassified knot types.

local action where a triangle pierced by one edge would be pierced in the other direction by a nearby edge), so one would expect the (2n+2)-gon to be a knot type with crossing number greater than the crossing number of the (2n)-gon most of the time. As such, any particular knot type eventually becomes "crowded out" by more complicated knot types at very large lengths.

Second, each knot type has a *stick number*, i.e. the smallest number of edges needed to create a polygon realizing that knot type, and the stick number has a lower bound that increases with crossing number [6]. So for edge numbers less than the stick number for that knot type, the given knot type is not even possible. At the stick number (or the stick number plus one, in case the value is odd) the knot type is barely possible. But as the number of edges increases, there is more flexibility in the available configurations forming this knot type, making it increasing probable.

The tension between these two ideas suggests that the probability peaks at some length, which differs depending on the knot type, seemingly with simpler knot types reaching the peak at lower numbers of edges.

Figure 13 shows the probability of knot types with crossing numbers 0 through 10. The cylindrical data curves are similar in shape to curves we computed for polygons under spherical confinement in [11]. In particular, the 0-crossing (unknot) data is always decreasing, beginning concave downward before hitting an inflection point and then decreasing concave upward to an asymptotic value of 0. For higher crossing numbers, the graph starts increasing concave upward, has an inflection point to turn concave downward, reaches a maximum, has another inflection point to turn concave upward, and then approaches an asymptotic value of 0.

For crossing numbers between 0 and 10, the behavior of the probability is not entirely ordered by crossing number. In Figure 13(a), the 4-crossing knot types, which consist of just the amphichiral 4_1 knot, has lower probability over most of the graph than the 5-crossing knot types, which includes 5_1 and 5_2 , both of which are chiral. In Figure 13(b), the 5-crossing knot types are more probable than the 6-crossing knot types prior to their peaks. However, the 8-crossing knot types are more probable than the 7-crossing knot types at most lengths, and the 10-crossing knot types are more probable than the 9-crossing knot types at most lengths. Thus, in this range, there is a real advantage to having an even crossing number, likely due to the even numbers of edges.

If we restrict our attention to just the odd (or just the even) crossing numbers, then we see the graphs of the knot types ordered by crossing number (Figure 14), at least prior to their peaks. Following their peaks, the probabilities dissipate at different rates. We do not have a good idea for how to predict the dissipation rates.

Even amongst the even crossing numbers in Figure 14(b), the 4-crossing knot types seem out of place. As mentioned above, the 4-crossing knot types contain only the amphichiral 4₁ knot. At 6-crossings, we see the first composite knot types (plus two chiral and one amphichiral knot type) and at 8-crossings we see the first nonalternating knot types. Furthermore, the number of knot types per crossing number increases exponentially with crossing number asymptotically [20, 40]. We expect that the higher peak for 6-crossing knots than for

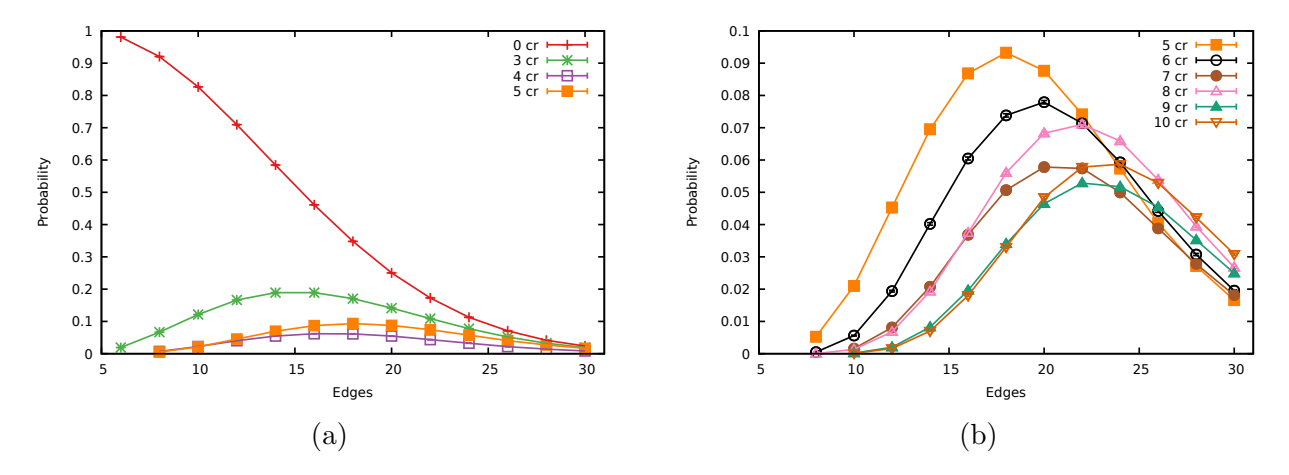


Figure 13: Probabilities of knot types in the cylindrical data with (a) crossing numbers between 0 and 5, and (b) crossing numbers between 5 and 10.

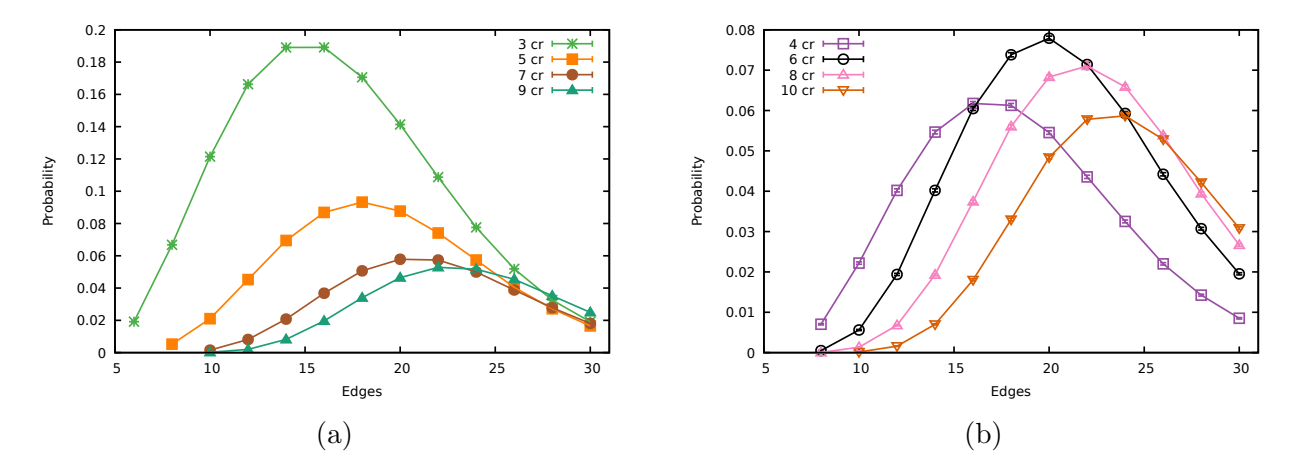


Figure 14: Probabilities for knot types in the cylindrical data with (a) odd crossing numbers: 3, 5, 7, and 9, and (b) even crossing numbers 4, 6, 8, and 10.

4-crossing knots is due to the additional knot types. For crossing numbers between 5 and 10 divided into even and odd crossing numbers, smaller crossing numbers have higher peaks and that peak occurs at smaller lengths.

Beyond 10 crossings, prior to their peaks, the combined probabilities of all knot types with a given crossing number are ordered simply by crossing number. Furthermore, the length at which such probabilities peak for a given crossing number is ordered by the crossing number. In Figure 15(a), we see this behavior. We also see that the probability graphs cross as the smaller crossing numbers are dissipating while the higher crossing numbers are just beginning to decrease. One can speculate that if we were to go to a polygonal length of 32 edges, the ordering of the probabilities would be inverted with respect to crossing number.

In Figure 15(b), we show the probability curves for the estimated crossing numbers 17 through 59, along with the 16-crossing probability data. The graph is stunningly uniform,

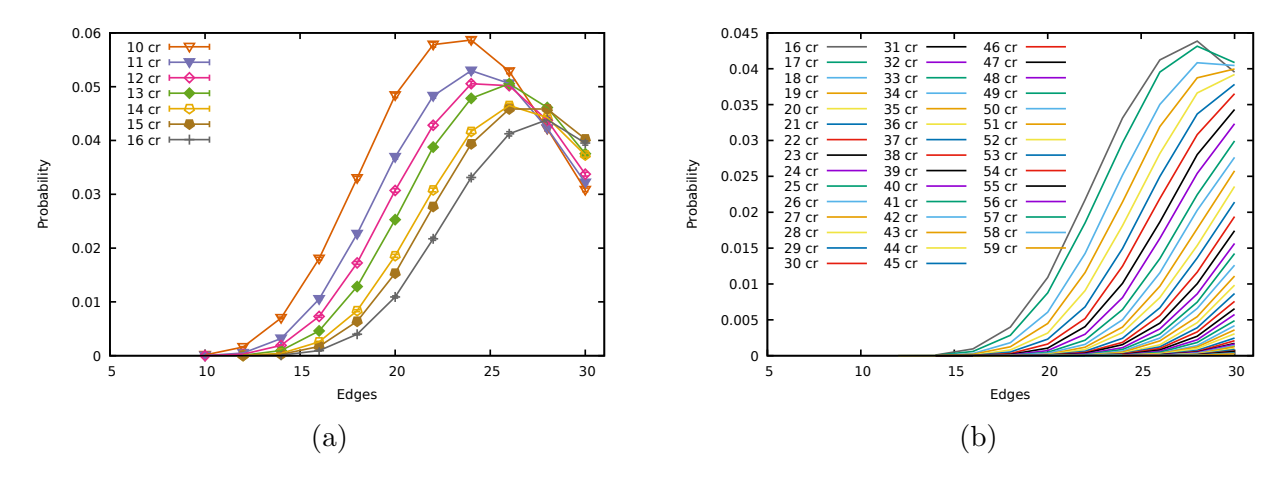


Figure 15: Probabilities for knot types in the cylindrical data with (a) crossing numbers between 10 and 16 and (b) crossing numbers between 16 and 59.

and suggests that our crossing number estimates within the unclassified knot types are really quite good. While the graph includes multiple repeats on colors, the take-home message is that the ordering by crossing number persists in this range, and one would expect to see the same "lower crossing number implies peaks at smaller numbers of edges" behavior to persist for all crossing numbers 10 and higher.

Furthermore, the graphs of Figure 15(a), and the graphs for crossing numbers 16 through 18 in Figure 15(b), show that the peak probability value decreases with increasing complexity. We believe this is because so many new knot types, and crossing numbers, become available with the addition of two new edges between cylinder knot lengths.

4.3 Probabilities of alternating knot types by crossing number

The alternating knot types show more regularity than the general probabilities seen in the previous section. In Figure 16(a), we show the probabilities of alternating knot types with crossing numbers between five and 10. Note that all of the 3-crossing and 4-crossing knot types are alternating knot types. We did not include the 3-crossing data since the probabilities are so much higher than the five through 10 crossing data, nor the 4-crossing data since we have already discussed its behavior. Also note that we do not have alternating versus nonalternating data for crossing numbers beyond 16 (i.e. within the unclassified data).

Within alternating knot types, the probability graphs are ordered simply by crossing number with lower crossing number implying that the peak is higher and it occurs at a smaller number of edges. In fact, the curves are perfectly ordered by crossing number prior to their peaks in both Figures 16(a) and Figure 16(b).

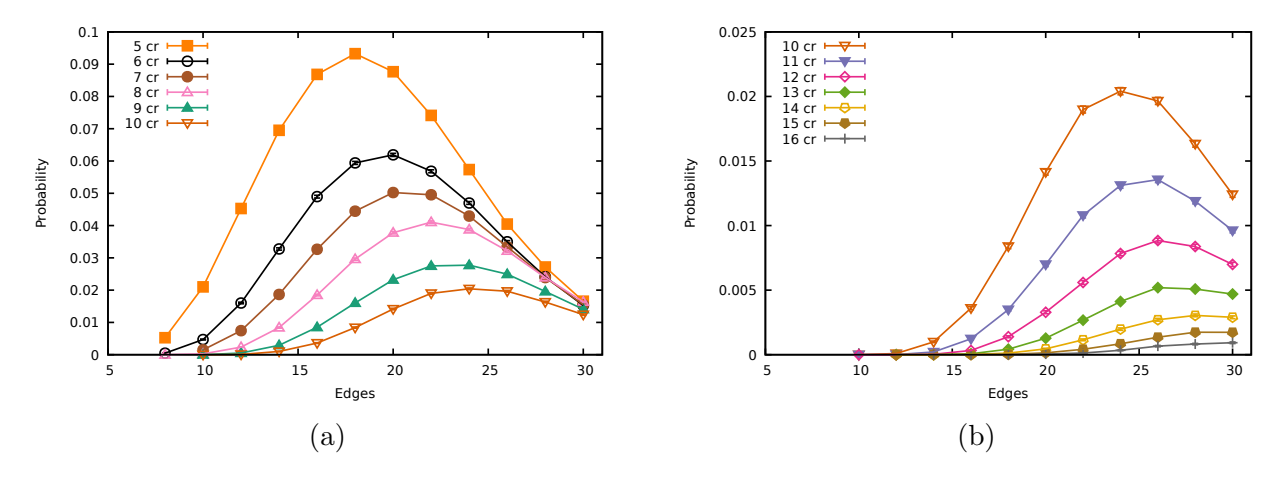


Figure 16: Probabilities for alternating prime knot types in the cylindrical data with (a) crossing numbers between 5 and 10, and (b) crossing numbers between 10 and 16.

4.4 Probabilities of nonalternating knot types by crossing number

The nonalternating probability data by crossing number (Figures 17 and 18) has a number of unusual features which help explain some of the full probability data in Section 4.2.

In Figure 17(a), we see anomalous behavior for nonalternating knot types with crossing numbers between eight and 10. The 8-crossing nonalternating knot types have a higher peak than the 9-crossing nonalternating knot types. Also, the 10-crossing knot types have higher probability than the 9-crossing knot types at all reported edges except 10 (0.000178 for 9-crossings versus 0.000135 for 10-crossings at 10 edges) and their peaks both occur at 22 edges.

In Figure 17(b), we see the behavior for nonalternating knot types between 10 and 16 crossings. We observe that the curves do not look as nicely ordered as the curves for alternating knots shown in Figure 16(b). To see the location of the peaks more clearly, we isolate the odd and even crossings numbers for nonalternating knot types in Figure 18. Within these groupings, we again see an ordering by crossing number with respect to peak probabilities and the position of the peak. We observe that the curves in Figure 17(b) are ordered by crossing number prior to their peak and seem mostly to be ordered again by crossing number at length 30. We also see that as the crossing number increases, the peak occurs a longer and longer lengths. The probability values of the peaks themselves increase up to 13 crossings. The probability values of the peaks from 13 to 15 crossings are all very similar. However the value for 16 crossings is slightly smaller. Thus we can speculate that with increasing crossing number the height of these peaks does not increase any further, and most likely declines, as was seen in Section 4.2.

From Table 4, we know that a very high percentage (at least 92%) of the knot types with crossing number exceeding 16 are nonalternating prime knot types. Therefore, if we were to plot the probability graphs for nonalternating knot types beyond 16 crossings, we would expect the graphs to look much like those in Figure 15(b) which contain all classes of knots

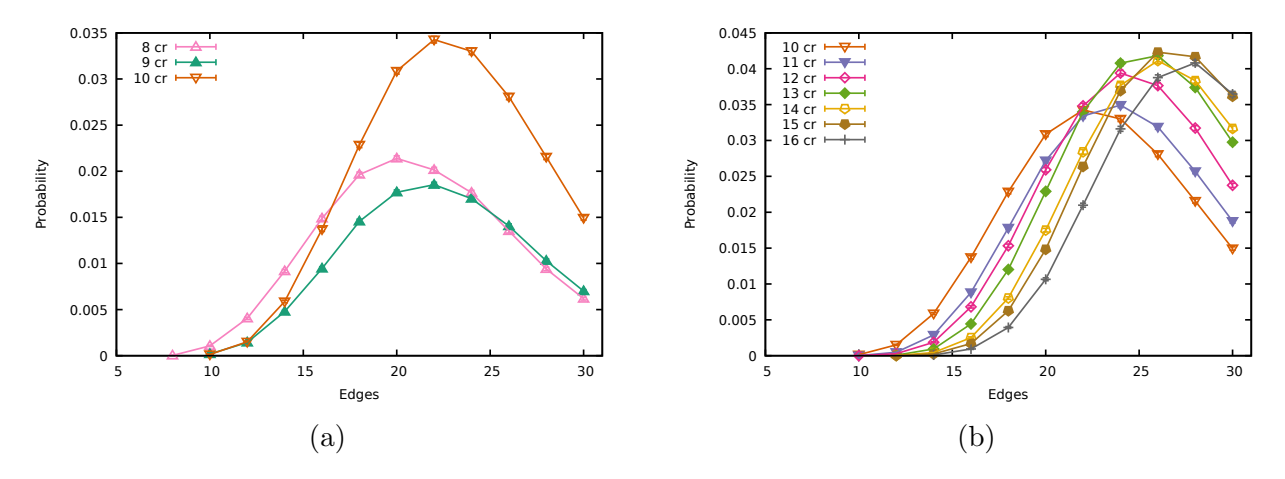


Figure 17: Probabilities for nonalternating prime knot types in the cylindrical data with (a) crossing numbers between 8 and 10, and (b) crossing numbers between 10 and 16.

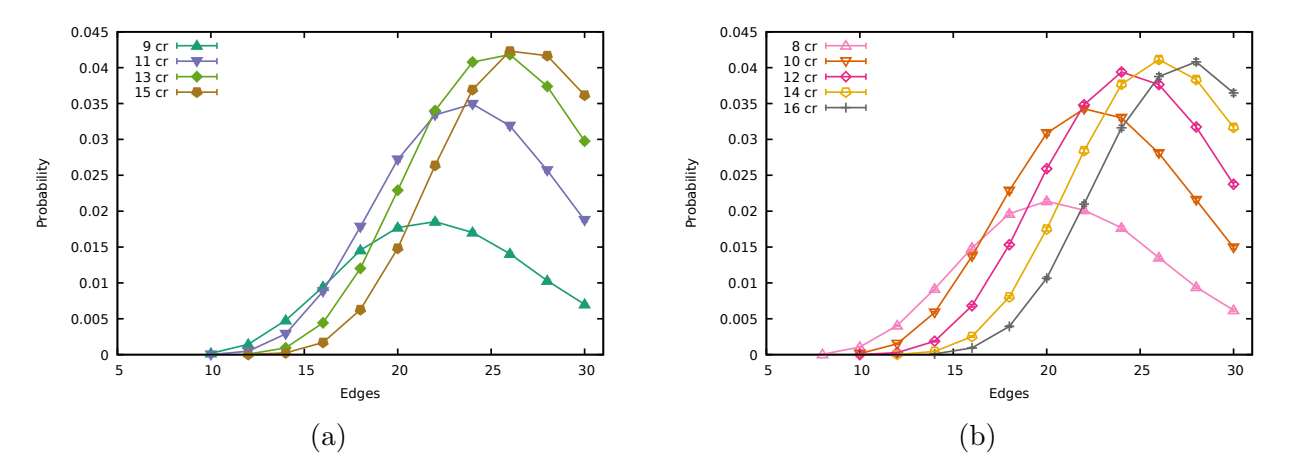


Figure 18: Probabilities for nonalternating knot types in the cylindrical data with (a) odd crossing numbers: 9, 11, 13, and 15, and (b) even crossing numbers: 8, 10, 12, 14, and 16.

with a given crossing number.

4.5 Probabilities of composite knot types by crossing number

The composite knot types, with the exception of the 7-crossing composite knot types, behave regularly. In Figure 19(a), we see that the 7-crossing composite knot types seem out of place. The 7-crossing composite knot types contain just two knot types $3_1\#4_1$ and its mirror image $m3_1\#4_1$, where 3_1 and $m3_1$ are mirror images. There are three 6-crossing composite knot types, $3_1\#3_1$, $3_1\#m3_1$, and $m3_1\#m3_1$, but recall that the 3_1 knot type, which includes both 3_1 and $m3_1$, has greater probability than the 4_1 . If we disregard the 7-crossing composite knot types, we again see that knot types with lower crossing number have higher peaks and those peaks appear at smaller lengths than higher crossing number knot types. This occurs

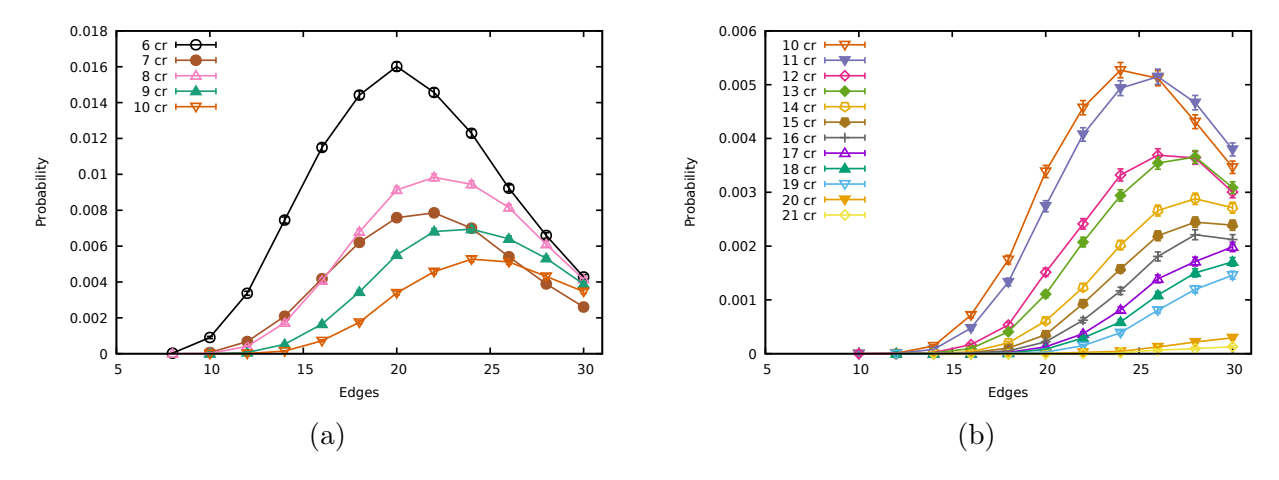


Figure 19: Probabilities for composite knot types in the cylindrical data with (a) crossing numbers between 6 and 10, and (b) crossing numbers between 10 and 16.

in both Figure 19(a) and Figure 19(b).

In Figure 19(b), we include the probabilities from the composite knots classified by knotfind with crossing number exceeding 16 from the unclassified knots. The results for 17, 18, and 19 crossings look consistent with the data for crossing numbers less than 17. However, there is a large gap between 19 and 20 crossings. For length 30 at 19 crossings there are 1459 configurations, of which 1091 are 3₁ knots composed with a 16-crossing knot type. At 20 crossings, then, we would expect a majority of the knot types to be 3₁ knots composed with 17-crossing knot types. But we do not classify the 17-crossing knot types with our software, so those configurations are considered unclassified. It could also be the case that knotfind is less and less effective at factoring composite with increasing crossing numbers, although we have no way of measuring to what extent this is true. To be fair, the software knotfind was not designed to optimize the factoring of composite knot types.

5 Summary

The configurations generated in the cylindrical model are independent of the ratio h/r where h is the cylinder height and r is the cylinder radius. Furthermore, they are not equilateral and not rooted at the origin – all the spherical polygons we generated earlier were equilateral and rooted at the origin. Still, our results show that the distribution of knot types of the polygons generated in the cylinder behave like the polygons under rooted spherical confinement with a confinement radius considerably smaller than one – estimated at an approximate confinement radius of R = 0.62. This suggests that both the rooting in the spherical model with values $R \geq 1$ and the non-equilateral nature of the cylindrical model do not greatly affect the distributions of knot types. Geometric quantities like average crossing number, curvature and torsion change depending on the ratio h/r and this will be the topic of a separate article.

For length 30, we find that the probabilities of unknotted and prime alternating knot

types in the cylindrical polygons decrease as $R \to 0.5^+$. We conjecture that the unknot probability approaches 0 and that the prime alternating probability approaches a positive value between 0.08 and 0.12. The composite knot types appear to approach a value around 0.065 as $R \to 0.5^+$, which leaves around 80% of the polygons to be nonalternating knot types.

We also analyze the cylindrical polygons as length increases. Unknotted polygons are already virtually extinct at length 30 while the probability of polygons representing a prime alternating knot type is initially increasing with a peak around 18 edges of 49% and then decreasing. At 30 edges still 16% of polygons represent alternating knot types, although we conjecture that this value approaches 0 as length increases. We conjecture that the composite knot types approach a value around 0.065 as length increases, which leaves around 93% of the polygons to be nonalternating knot types as $L \to \infty$.

Acknowledgments

This work was supported by the National Science Foundation grant number 1418869 and 1720342 to EJR.

References

- [1] C. Adams. The Knot Book: An elementary introduction to the mathematical theory of knots. American Mathematical Society, 2004.
- [2] Javier Arsuaga, Mariel Vazquez, Paul McGuirk, Sonia Trigueros, De Witt Sumners, and Joaquim Roca. DNA knots reveal a chiral organization of DNA in phage capsids. *Proc. Natl. Acad. Sci. USA*, 102(26):9165–9169, 2005.
- [3] Javier Arsuaga, Mariel Vázquez, Sonia Trigueros, De Witt Sumners, and Joaquim Roca. Knotting probability of DNA molecules confined in restricted volumes: DNA knotting in phage capsids. *Proc. Natl. Acad. Sci. USA*, 99:5373–5377, 2002.
- [4] Gerhard Burde and Heiner Zieschang. Knots, volume 5 of De Gruyter Studies in Mathematics. Walter de Gruyter & Co., Berlin, second edition, 2003.
- [5] Benjamin A. Burton. The next 350 million knots. In Sergio Cabello and Danny Z. Chen, editors, 36th International Symposium on Computational Geometry (SoCG 2020), volume 164 of Leibniz International Proceedings in Informatics (LIPIcs), pages 25:1–25:17, Dagstuhl, Germany, 2020. Schloss Dagstuhl-Leibniz-Zentrum für Informatik.
- [6] Jorge Alberto Calvo. Geometric knot spaces and polygonal isotopy. *J. Knot Theory Ramifications*, 10(2):245–267, 2001. Knots in Hellas '98, Vol. 2 (Delphi).
- [7] Jason Cantarella and Clayton Shonkwiler. The symplectic geometry of closed equilateral random walks in 3-space. *Ann. Appl. Probab.*, 26(1):549–596, 2016.

- [8] Marc Culler, Nathan M. Dunfield, Matthias Goerner, and Jeffrey R. Weeks. SnapPy, a computer program for studying the geometry and topology of 3-manifolds. Available at http://snappy.computop.org.
- [9] Pawel Dabrowski-Tumanski, Pawel Rubach, Dimos Goundaroulis, Julien Dorier, Piotr Sułkowski, Kenneth C Millett, Eric J Rawdon, Andrzej Stasiak, and Joanna I Sułkowska. KnotProt 2.0: a database of proteins with knots and other entangled structures. *Nucleic Acids Res.*, 47(D1):D367–D375, 12 2018.
- [10] Yuanan Diao. The knotting of equilateral polygons in \mathbb{R}^3 . J. Knot Theory Ramifications, $4(2):189-196,\ 1995.$
- [11] Yuanan Diao, Claus Ernst, Anthony Montemayor, Eric Rawdon, and Uta Ziegler. The knot spectrum of confined random equilateral polygons. *Mol. Based Math. Biol.*, 2(1):19–33, 2014.
- [12] Yuanan Diao, Claus Ernst, Anthony Montemayor, and Uta Ziegler. Generating equilateral random polygons in confinement. J. Phys. A: Math. Theor., 44:405202, 2011.
- [13] Yuanan Diao, Claus Ernst, Anthony Montemayor, and Uta Ziegler. Generating equilateral random polygons in confinement II. J. Phys. A: Math. Theor., 45:275203, 2012.
- [14] Yuanan Diao, Claus Ernst, Anthony Montemayor, and Uta Ziegler. Generating equilateral random polygons in confinement III. J. Phys. A: Math. Theor., 45:465003, 2012.
- [15] Yuanan Diao, Claus Ernst, Eric J. Rawdon, and Uta Ziegler. Average crossing number and writhe of knotted random polygons in confinement. *React. Funct. Polym.*, 131:430– 444, 2018.
- [16] Yuanan Diao, Claus Ernst, Eric J. Rawdon, and Uta Ziegler. Relative frequencies of alternating and nonalternating prime knots and composite knots in random knot spaces. *Exp. Math.*, 27(4):454–471, 2018.
- [17] Yuanan Diao, Claus Ernst, Eric J. Rawdon, and Uta Ziegler. Total curvature and total torsion of knotted random polygons in confinement. *J. Phys. A: Math. Theor.*, 51(15):154002, 2018.
- [18] Yuanan Diao, Claus Ernst, Uta Ziegler, and Eric J. Rawdon. The knot spectrum of random knot spaces. In Philipp Reiter, Simon Blatt, and Armin Schikorra, editors, New Directions in Geometric and Applied Knot Theory. De Gruyter, Berlin, 2018.
- [19] D. B. A. Epstein and R. C. Penner. Euclidean decompositions of noncompact hyperbolic manifolds. *J. Differential Geom.*, 27(1):67–80, 1988.
- [20] C. Ernst and D. W. Sumners. The growth of the number of prime knots. *Math. Proc. Cambridge Philos. Soc.*, 102(2):303–315, 1987.

- [21] Claus Ernst, Uta Ziegler, and Eric J. Rawdon. Configurations and knot types of random cylindrical knots used to model knotting in extreme confinement [dataset]. https://ir.stthomas.edu/cas_mathpub/5/.
- [22] Claus Ernst, Uta Ziegler, and Eric J. Rawdon. Configurations and knot types of random equilateral rooted polygons under spherical confinement with (a) 30 edges and radii between 1.0 and 4.5, and (b) radius 3.0 and edges between 10 and 90 [dataset]. https://ir.stthomas.edu/cas_mathpub/4/.
- [23] Claus Ernst, Uta Ziegler, and Eric J. Rawdon. Configurations and knot types of random equilateral rooted polygons under spherical confinement with between 10 and 90 edges and radii between 1.0 and 4.5 [dataset]. https://ir.stthomas.edu/cas_mathpub/3/.
- [24] Bruce Ewing and Kenneth C. Millett. Computational algorithms and the complexity of link polynomials. In *Progress in knot theory and related topics*, pages 51–68. Hermann, Paris, 1997.
- [25] P. Freyd, D. Yetter, J. Hoste, W. B. R. Lickorish, K. Millett, and A. Ocneanu. A new polynomial invariant of knots and links. *Bull. Amer. Math. Soc.* (N.S.), 12(2):239–246, 1985.
- [26] Mark Galassi, Jim Davies, James Theiler, Brian Gough, Gerard Jungman, Patrick Alken, Michael Booth, and Fabrice Rossi. *GNU Scientific Library Reference Manual*. Network Theory Ltd., third edition, 2009. Software available at http://www.gnu.org/software/gsl/.
- [27] Jim Hoste and Morwen Thistlethwaite. Knotscape. http://www.math.utk.edu/~morwen/knotscape.html. Program for computing topological information about knots.
- [28] Jim Hoste, Morwen Thistlethwaite, and Jeff Weeks. The first 1,701,936 knots. *Math. Intelligencer*, 20(4):33–48, 1998.
- [29] P. J. Jardine and D. L. Anderson. Dna packaging in double-stranded dna phages. In Richard Calendar, editor, *The bacteriophages*, pages 49–65. Oxford University Press, 2006.
- [30] Akio Kawauchi. A Survey of Knot Theory. Birkhäuser Verlag, Basel, 1996.
- [31] Zhirong Liu and Hue Sun Chan. Efficient chain moves for monte carlo simulations of a wormlike dna model: Excluded volume, supercoils, site juxtapositions, knots, and comparisons with random-flight and lattice models. *J. Chem. Phys.*, 128(14):145104, 2008.
- [32] Charles Livingston. Knot theory, volume 24. Cambridge University Press, 1993.

- [33] D Marenduzzo, C Micheletti, and E Orlandini. Biopolymer organization upon confinement. J. Phys. Condens. Matter, 22(28):283102, jun 2010.
- [34] C. Micheletti, D. Marenduzzo, E. Orlandini, and D. W. Summers. Knotting of random ring polymers in confined spaces. *J. Chem. Phys.*, 124(6):064903, 2006.
- [35] C. Micheletti, D. Marenduzzo, E. Orlandini, and D.W. Sumners. Simulations of knotting in confined circular dna. *Biophys. J.*, 95(8):3591 3599, 2008.
- [36] Nicholas Pippenger. Knots in random walks. Discrete Appl. Math., 25(3):273–278, 1989.
- [37] Józef H. Przytycki and Paweł Traczyk. Invariants of links of Conway type. *Kobe J. Math.*, 4(2):115–139, 1987.
- [38] Richard Randell. An elementary invariant of knots. *J. Knot Theory Ramifications*, 3(3):279–286, 1994. Random knotting and linking (Vancouver, BC, 1993).
- [39] D. W. Sumners and S. G. Whittington. Knots in self-avoiding walks. J. Phys. A: Math. Theor., 21(7):1689–1694, 1988.
- [40] Carl Sundberg and Morwen Thistlethwaite. The rate of growth of the number of prime alternating links and tangles. *Pacific J. Math.*, 182(2):329–358, 1998.
- [41] Morwen Thistlethwaite. unraveller, 2009. Software to simplify knot diagrams.
- [42] Luca Tubiana, Enzo Orlandini, and Cristian Micheletti. Multiscale entanglement in ring polymers under spherical confinement. *Phys. Rev. Lett.*, 107:188302, Oct 2011.
- [43] A. V. Vologodskii, S. D. Levene, K. V. Klenin, M. D. Frank-Kamenetskii, and N. R. Cozzarelli. Conformational and thermodynamic properties of supercoiled DNA. J. Mol. Biol., 227:1224–1243, 1992.